


RESEARCH ARTICLE

Measuring chemical exchange saturation transfer exchange rates in the human brain using a particle swarm optimisation algorithm

Andrew J. Carradus | Joe M. P. Bradley | Penny A. Gowland | Olivier E. Mougin 

Sir Peter Mansfield Imaging Centre and NIHR Nottingham Biomedical Research Centre, Nottingham University Hospitals NHS Trust, School of Physics and Astronomy, University of Nottingham, Nottingham, UK

Correspondence

Olivier E. Mougin, Sir Peter Mansfield Imaging Centre and NIHR Nottingham Biomedical Research Centre, Nottingham University Hospitals NHS Trust, School of Physics and Astronomy, University of Nottingham, Nottingham, UK.
Email: olivier.mougin@nottingham.ac.uk

Funding information

Haydn Green Foundation

Abstract

The z-spectrum contains many pools with different exchange rates and T_2 values, which can make it difficult to interpret in vivo data and complicates the design of experiments aimed at providing sensitivity to one pool. This work aims to characterise the main pools observable with MRI at 7T in the human brain. To achieve this, we acquired z-spectra at multiple saturation powers in the human brain at 7T. We used simulations to optimise the use of particle swarm optimisation (PSO) to fit these data, validating this approach using further simulations and creatine phantoms. We then used the PSO to fit data from grey and white matter for the pool size, exchange rate, and T_2 of five proton pools (magnetisation transfer, amides, amines, nuclear Overhauser enhancement $\text{NOE}_{-3.5\text{ppm}}$ and $\text{NOE}_{-1.7\text{ppm}}$ in addition to water). We then devised an approach for using PSO to fit z-spectra while limiting the computational burden, and we investigated the sensitivity of the fit to T_2 and k for three overlapping pools. We used this to measure the exchange rate of creatine and to show that it varied with temperature, as expected. In the brain we measured a significantly larger pool size in white matter than in grey matter for the magnetisation transfer pool and the $\text{NOE}_{-3.5\text{ppm}}$ pool. For all other parameters we found no significant difference between grey and white matter. We showed that PSO can be used to fit z-spectra acquired at a range of B_1 to provide information about peak position, amplitude, exchange rate, and T_2 in vivo in the human brain. These data could provide more sensitivity to change in some clinical conditions and will also provide key information for further experimental design.

KEYWORDS

amides, amines, CEST, magnetisation transfer, NOE, z-spectrum

Abbreviations: CEST, chemical exchange saturation transfer; CW, continuous wave; GM, grey matter; MT, magnetisation transfer; NOE, nuclear Overhauser enhancement; PSIR, phase-sensitive inversion recovery; PSO, particle swarm optimisation; QUESP, quantifying exchange rates using varying saturation power; QUEST, quantifying exchange rates using varying saturation time; WM, white matter; z-PSO, z-spectra PSO.

This is an open access article under the terms of the [Creative Commons Attribution-NonCommercial](https://creativecommons.org/licenses/by-nc/4.0/) License, which permits use, distribution and reproduction in any medium, provided the original work is properly cited and is not used for commercial purposes.

© 2023 The Authors. *NMR in Biomedicine* published by John Wiley & Sons Ltd.

1 | INTRODUCTION

In MRI, the z-spectrum represents the change in water signal due to its exchange with off-resonance magnetisation and yields information about solute molecules present in a sample through magnetisation transfer (MT), chemical exchange saturation transfer (CEST), and nuclear Overhauser enhancements (NOEs) thought to be mediated through chemical exchange. However, the size and shape of each peak in the z-spectrum depends not only on the concentration of exchanging solute, but also on the rate at which it exchanges with the water protons and its T_2 . The exchange rate is of particular interest biologically because it is generally pH dependent,¹ and for experimental design because the relationship between the CEST signal and saturation power depends on the exchange rate. However, there remains considerable uncertainty in the values of these basic biological parameters in human tissues.

Analytical solutions exist to the Bloch–McConnell equations (which provide a complete description of precession, relaxation, and exchange in a multipool system) and these have been used to estimate either pool size² or exchange rate,³ but are unable to separate these parameters directly.⁴ Experimental approaches have been proposed to measure exchange rates including QUESP and QUEST (quantifying exchange rates using varying saturation power and time, respectively) methods.⁵ Of these, only QUESP is capable of truly separating pool size and exchange rate,⁶ but a reasonable estimate of exchange rate is required prior to the experiment, because saturation power must be optimally sampled around k/γ , and QUESP may become invalid in the case of overlapping CEST peaks. An alternative approach is to collect z-spectra at a range of saturation powers and fit directly for pool size and exchange rate, which will account for overlapping peaks, but which is computationally very expensive. One solution is to compare acquired spectra with a look-up table of z-spectra simulated for a range of pool sizes, exchange rates, and apparent T_2 for each exchanging pool at different saturation powers.^{7–9} This requires prior knowledge of the system, because the fitted variables must lie within in the range of variables simulated in the look-up table, and although computationally efficient, it imposes large memory requirements. Alternatively, z-spectra can be fitted using a Bayesian approach,¹⁰ which drastically reduces the computation time, but the results can be biased if the estimated Bayesian priors are incorrect.

Here, we present a novel method of fitting the z-spectrum to measure the pool size and exchange rate of exchanging CEST and NOE pools with, we believe, fewer assumptions than any currently reported method, by using a particle swarm optimisation (PSO) algorithm to search variable space for the solutions for the Bloch–McConnell equations, while avoiding local minima. This paper describes tests of the PSO fit in simulations and creatine phantoms, and then describes work undertaken using the PSO to investigate the number of pools needed to characterise the z-spectrum from grey matter (GM) and white matter (WM) in vivo at 7T.

2 | THEORY

2.1 | Particle swarm optimisation for fitting z-spectra

Fitting the z-spectrum poses two challenges: changes in the size, exchange rate, and apparent T_2 of a pool can produce similar effects on the shape of a z-spectrum, and the effects of overlapping peaks combine nonlinearly. The PSO algorithm^{11,12} is particularly appropriate for solving highly nonlinear, multidimensional problems¹³ which lead to local minima.

Broadly, the PSO algorithm initialises a ‘swarm’ of particles, each with random coordinates and random velocity within the bounded variable space. The velocities determine the changes in particle positions between iterations. A minimisation function is used to calculate how close each particle is to the optimal solution (‘best position’) at each iteration. For each iteration the velocity of a particle is determined by where it is currently going, the best place it has been, and the best place any particle currently is. Formally, the velocity of particle i at $k+1$ th iteration is given by

$$\mathbf{v}_{k+1}^i = w\mathbf{v}_k^i + c_1 \text{rand} \frac{\mathbf{p}^i - \mathbf{x}_k^i}{\Delta t} + c_2 \text{rand} \frac{\mathbf{p}_k^g - \mathbf{x}_k^i}{\Delta t}, \quad (1)$$

where \mathbf{x}_k^i is the position of particle i in the current iteration k , \mathbf{v}_k^i is the velocity of particle i in the k th iteration, rand is the random function, \mathbf{p}^i is the best position of particle i from all previous iterations, and \mathbf{p}_k^g is the position of the g th particle that is in the best position during the current k th iteration. The inertia factor, w , controls the influence of current motion on subsequent particle velocity (usual range between 0.4 and 1.4); the self-confidence range, c_1 , controls the influence of individual particle history on subsequent particle velocity (usual range between 1.5 and 2); and the swarm confidence range, c_2 , controls the influence of the swarm history on subsequent particle velocity (usual range between 2 and 2.5).¹⁴ Figure 1 illustrates the PSO algorithm for a one-dimensional problem with several local minima.

An analytical, steady state, solution to the Bloch–McConnell equations describing the effect of continuous wave (CW) saturation was used to simulate the z-spectra^{2,15}:

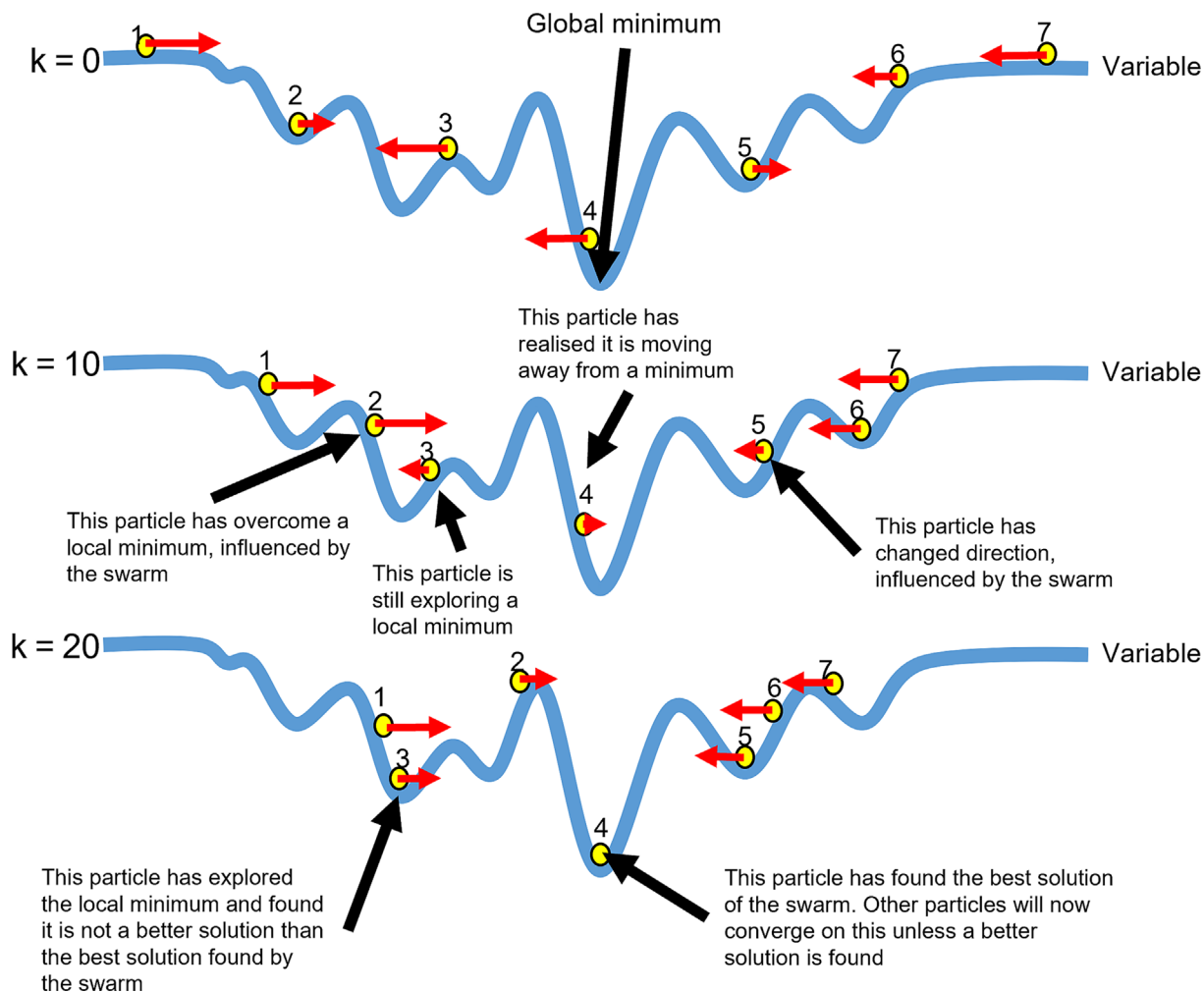


FIGURE 1 Illustration of how the PSO works, showing evolution of the seven particles to solve a one-dimensional problem with multiple local minima, from initialisation ($k = 0$), to $k = 10$ and $k = 20$ iterations (at which point the problem was solved). PSO, particle swarm optimisation.

$$Z(\Delta\omega, t) = (\cos^2(\theta) - Z(\Delta\omega)_{ss})e^{-\frac{t}{T_{1,\rho}}} + Z_{ss}, \quad (2)$$

where Z_{ss} is the steady state condition, $T_{1,\rho}$ is the overall longitudinal relaxation time of the system in the rotating frame, t_{sat} is the length of time that saturation is applied for, and θ is the angle between the effective field during saturation and the z direction in the rotating frame, $\theta = \tan^{-1} \frac{\omega_1}{\Delta\omega}$, where $\omega_1 = \gamma B_1$. $R_{1,\rho}$ at a particular off-resonant frequency ($\Delta\omega$) is given by

$$R_{1,\rho}(\Delta\omega) = R_{eff}(\Delta\omega) + R_{ex,b}(\Delta\omega) + R_{ex,c}(\Delta\omega) + R_{ex,n}(\Delta\omega) \quad (3)$$

when considering four pools: free water, a bound pool (b), a CEST pool centred on +3.5 ppm (c), and an NOE pool centred on -3.5 ppm (n), although this can easily be generalised to more pools. $R_{eff}(\Delta\omega)$ describes the relaxation of free water in the rotating frame:

$$R_{eff}(\Delta\omega) = R_{1,f} \cos^2\theta + R_{2,f} \sin^2\theta \quad (4)$$

$R_{ex,i}$ for a general exchanging pool, i , is assumed to have a line shape that can be expressed as¹⁵

$$R_{ex,i}(\Delta\omega) = M_{0,i} k_i \frac{A_i(\Delta\omega)}{\frac{\Gamma_i^2}{4} + (\Delta\omega - \delta\omega_i)^2}, \quad (5)$$

where the full width half maximum is given by

$$\Gamma_i = 2\sqrt{\omega_1^2 \frac{k_i + R_{2,i}}{k_i} + (k_i + R_{2,i})^2} \quad (6)$$

and

$$A_i(\Delta\omega) = \frac{\omega_1^2}{(\Delta\omega^2 + \omega_1^2)} \cdot \left(\delta\omega_i + \frac{R_{2,i}(\Delta\omega^2 + \omega_1^2)}{k_i} + R_{2,i}(k_i + R_{2,i}) \right). \quad (7)$$

$M_{0,i}$ is the size of the i^{th} pool expressed as a fraction of the total proton pool, k_i is its exchange rate with water in Hz, $T_{2,i}$ is its apparent transverse relaxation time in seconds, and $\delta\omega_i$ is its frequency offset in Hz. The MT bound pool (b) line shape cannot be defined analytically, but the analysis above assumes that it can be approximated as a Lorentzian close to the water resonance¹⁶; the result of this is that the estimated values of k_b and $T_{2,b}$ are only indicators of the underlying macromolecular bound pool.² Experimental z-spectra acquired at multiple off-resonant frequencies ($\Delta\omega$) and a range of saturation amplitudes (ω_1), using CW saturation with a saturation time exceeding $T_{1,f}/4$ to reach steady state, can be fitted for $M_{0,i}$, k_i , $T_{2,i}$ and $\delta\omega_i$ of each pool using the PSO algorithm. The prior information required is the expected number of exchanging pools, their frequency offsets ($\delta\omega_i$, allowed to vary by 0.1 ppm), the B_1 values for each level of saturation estimated from B_1 maps, the saturation time, and the observed T_1 .

Fitting multiple parameters together is very time consuming, therefore, a multilevel recursive fitting approach was developed for multipool fits, first fitting each exchanging pool to a limited range of the z-spectrum data, before finally fitting all pools to the whole spectrum together. This is described in the Methods for the human brain data.

3 | METHODS

Initially, the method of applying the PSO to fit z-spectra (z-PSO) was optimised. Then Monte Carlo simulations were performed to investigate the accuracy and precision of the fit. Next, z-PSO was used to investigate the effect of temperature and pH on the exchange rate in a creatine phantom. Finally, the z-PSO was used to measure the z-spectrum parameters in the human brain.

3.1 | z-PSO optimisation

Experimental z-spectra acquired from cerebral GM at 63 off-resonance frequencies (indicated in Table 1) and at five saturation powers were fitted to a six-pool model (free water, MT, amides, $\text{NOE}_{-3.5\text{ppm}}$, $\text{NOE}_{-1.7\text{ppm}}$ and amines). The PSO was run for a varying number of particles, computation time was recorded, and the final sum of squares difference between the data and fitted spectra was used as a metric of goodness of fit (Figure 2A). Fits containing smaller numbers of particles were then repeated so that the number of particles multiplied by the number of repeats equalled 100,000 (Figure 2B shows 100 repeats of a swarm of 1000 particles) and the best fit across all repeats was then taken for each swarm size (Figure 2C).

Simulations were used to determine the potential precision and accuracy of the fitting. z-spectra were simulated with one exchanging amide pool located at +3.5 ppm, sampled at 63 off-resonance frequencies and at five saturation powers. Twenty-seven sets of spectra were simulated, with varying combinations of pool size (0.1%, 0.5%, and 1.0%), exchange rate (10, 100, and 1000 Hz), and T_2 (1, 10, and 100 ms). Gaussian noise was added to each spectral point, at a level representative of experimental data (0.5% of $M_{0,f}$), and this was repeated to give 10 realisations of each spectrum. Each spectrum was fitted using z-PSO.

Next, to determine how the fitting of exchanging pools was affected by the presence of an underlying MT pool, this was repeated for a three-pool model (free water, MT, and one CEST pool located at +3.5 ppm), with the CEST pool parameters fixed at $M_{0,c} = 1\%$, $k_c = 100$ Hz, and $T_{2,c} = 10$ ms, and the bound pool parameters varying as $M_{0,b} = 1\%$, 5%, and 10%, $k_b = 1, 10$, and 100 Hz, and $T_{2,b} = 50, 100$, and 200 μs .

3.2 | Creatine phantoms

Creatine phantoms were used to investigate the feasibility of using z-PSO to find the exchange rate, as the creatine signal at +2.0 ppm¹⁷ has an exchange rate that depends on both temperature and pH.¹⁸ Creatine solutions (10 g/L) with pH 5.5, 7.0, and 8.5 were created by adding

TABLE 1 Indicating how progressive z-PSO fits included different pools and data at different frequencies in the z-spectra, in a multilevel recursive approach to multipool model fitting.

Pools fitted		Frequency of datapoints used in fit	
MT and free water	Fit	1	2
	1	✓	✓
	2	✓	✓
	3	✓	✓
	4	✓	✓
	5	✓	✓
	6	✓	✓
	7	✓	✓
	8	✓	✓
	9	✓	✓
	10	✓	✓
	11	✓	✓
T1obs and T2f		✓	✓
amines			✓
NOE -1.7 ppm			✓
NOE -3.5ppm		✓	✓
Amides		✓	✓
		333.3	✓
		66.7	✓
		33.3	✓
		30.0	✓
		23.3	✓
		16.7	✓
		10.0	✓
		6.7	✓
		5.7	✓
		5.0	✓
		4.7	✗
		4.3	✗
		4.0	✗
		3.8	✗
		3.7	✗
		3.5	✗
		3.3	✗
		3.2	✗
		3.0	✗
		2.7	✗
		2.3	✗
		2.2	✗
		2.0	✗
		1.8	✗
		1.7	✗
		1.5	✗
		1.3	✗
		1.2	✗
		0.8	✓
		0.3	✓
		0.2	✓
		0.0	✓
		-0.2	✓
		-0.3	✓
		-0.8	✓
		-1.2	✗
		-1.3	✗
		-1.5	✗
		-1.7	✗
		-1.8	✗
		-2.0	✗
		-2.2	✗
		-2.3	✗
		-2.7	✗
		-3.0	✗
		-3.2	✗
		-3.3	✗
		-3.5	✗
		-3.7	✗
		-3.8	✗
		-4.0	✗
		-4.3	✗
		-4.7	✗
		-5.0	✓
		-5.7	✓
		-6.7	✓
		-10.0	✓
		-16.7	✓
		-23.3	✓
		-30.0	✓
		-33.3	✓
		-66.7	✓
		-333.3	✓

✓ fit this pool.
 ▼ use parameters from previous fit for this pool.
 y include this datapoint in the fit.
 n exclude this datapoint from the fit.

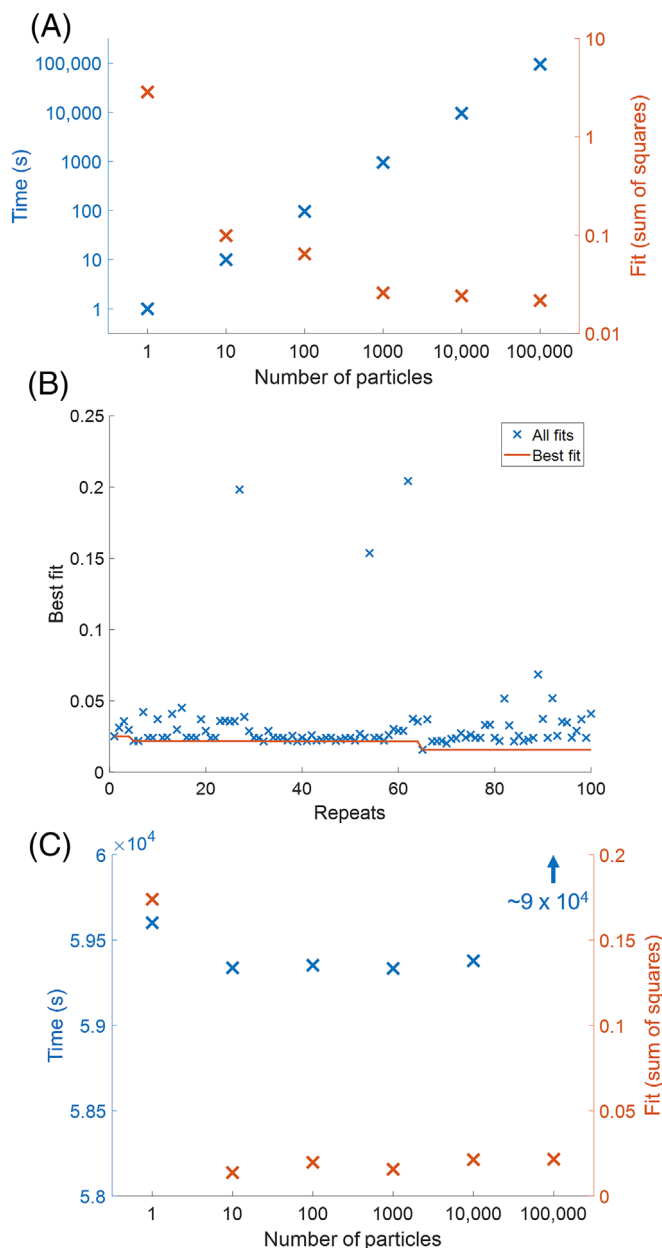


FIGURE 2 (A) Variation in goodness of fit (final sum of squares) and computation time for the final PSO fit, using swarm of different sizes. (B) The change in best goodness of fit (considering all fits so far) for 100 repeats of a swarm of 1000 particles, so that the total number of particles considered was 100,000. (C) Variation in goodness of fit and computation time when using swarms of different sizes repeated to give a total number of particles of 100,000, and then choosing the best fit from each of the sub fits as in (B). PSO, particle swarm optimisation.

phosphate buffer solution (sodium chloride solution containing a combination of monosodium phosphate and disodium phosphate in different proportions for different pHs). Six millilitres of each solution was placed into a sealed test tube, which was placed in an MR-compatible water bath inside the NOVA eight-channel pTx head coil of a 7T Philips Achieva MRI system. The water bath was connected to heated/cooled water pumped via tubes fed through the wave guides in the RF cage of the scanner room. The water bath was heated/cooled to the target temperature then switched off and allowed to settle for 2 min before scanning to avoid residual flow artefacts. The pump was switched back on between the acquisition of each spectrum, to bring the water bath back to the target temperature (at 40°C the bath cooled by 1–2°C during the acquisition of each spectrum).

Because of hardware limitations, semi-CW saturation had to be used,¹⁹ in which odd/even channels on the pTx system transmit were alternately driven with 50-ms square pulses for a total of 3 s. The RF power to the odd and even channels was adjusted to give similar B_1 in a central region of interest (ROI) of the sample. Final B_0 and B_1 maps were then acquired. Z-spectra were acquired at 64 off-resonance frequencies between $\pm 100,000$ Hz with a 3-s saturation train comprised of 60 alternating odd/even channel RF blocks of 50 ms, for $B_{1,\max}$ of 0.5, 1.0, and

1.5 μ T. The acquisition of each z-spectrum took 9.5 min using a turbo field echo (TFE)-echo planar imaging (EPI) readout (TFE factor 102 in-plane, EPI factor 11 in slice, TR = 17 ms, TE = 8 ms, shot-to-shot interval = 9 s [made up of 3 s of saturation, 1.7 s of readout, and 4.3 s of recovery], SENSE 2, $1 \times 1 \times 3$ mm³ voxels). This was repeated with the water bath at 40, 30, 20, and 10°C.

The data were processed using in-house functions written in MATLAB.²⁰ The first acquired point in each z-spectrum was discarded, because of the system approaching steady-state. The spectra were B_0 -corrected by shifting the z-spectrum from each pixel by the value of the field offset in the corresponding pixel in the acquired B_0 map and then interpolating to the original sampling points. Next, the data were normalised by dividing each point in the z-spectrum by the point acquired at +100,000 Hz, which was equivalent to the signal acquired after no saturation (S_0), assuming there are no exchanging pools this far off resonance.^{9,21} The average signal within each sample (at each temperature and pH) was calculated to give z-spectra at three different saturation powers, which were finally fitted to a two-pool model with $\delta\omega_c$ allowed to vary between +1.85 and +2.15 ppm, $M_{0,c}$ allowed to vary between 0% and 0.5%, k_c allowed to vary between 1 and 2000 Hz, and $T_{2,c}$ allowed to vary between 0.5 and 100 ms. $T_{1,obs}$ was fitted from the change in on-resonance signal away from the creatine peak with RF saturation. The z-PSO used a swarm of 20,000 particles, run 100 times (180 min for 100 runs) to fit the two-pool model, with the points around the visible peaks upweighted in the fit to avoid overfitting noise in the wings of the spectra at low temperature where the exchanging peaks were small.

3.3 | Human brain tissue in vivo

Six healthy volunteers (four females; age 24 ± 1 years) were recruited and scanned in the 7T Philips Achieva MRI scanner using a NOVA eight-channel pTx head coil, once local ethical approval had been received and each participant had provided written consent. The same sequence was used to acquire the z-spectrum as for the creatine phantom, except that this time, spectra were acquired at 63 off-resonance points and at five nominal B_1 values of 0.33, 0.67, 1.00, 1.33, and 1.67 μ T. A $192 \times 192 \times 24$ mm three-dimensional acquisition volume was positioned above the ventricles using the sequence described for the creatine phantom. Subjects were encouraged to watch a movie through prism glasses during the scan, to alleviate boredom and reduce head motion.²² A high-resolution T_1 -weighted anatomical image (phase-sensitive inversion recovery [PSIR]²³) was acquired to create GM and WM masks using FAST (FMRIB's Automated Segmentation Tool)²⁴ excluding pixels on the GM/WM boundary. B_1 and B_0 maps were acquired using the AFI sequence and a multigradient echo sequence. After acquisition, the z-spectrum images were coregistered using MCFLIRT (intramodal Motion Correction based on FMRIB's Linear Image Registration Tool)²⁵ and then the whole dataset was aligned to the PSIR image using FLIRT (FMRIB's Linear Image Registration Tool). The data were B_0 -corrected by interpolation based on the B_0 map. The data from the z-spectrum images were averaged over the masks to create a set of spectra for the GM and WM for each subject. The average value of B_1 across the masks was also calculated for each subject.

The GM and WM spectra for each subject were fitted using z-PSO to a six-pool model including (offset frequency with bounds) free water (0 ppm), MT (-2.34 ± 0.05 ppm), amides ($+3.5 \pm 0.1$ ppm), amines ($+2.0 \pm 0.15$ ppm), NOE (-3.5 ± 0.1 ppm), and a second NOE (-1.7 ± 0.15 ppm, as previously observed in blood⁹ and rat brain²⁶). These peaks were selected based on the literature and the peaks observed in the acquired spectra. A multilevel recursive fitting approach was used to fit these six-pool data, initially fitting each exchanging pool to a limited range of the spectrum, before finally fitting all pools to the whole spectrum together (Table 1). First, the acquired z-spectra (excluding points in the ranges of -5 to -1 ppm, and +1 to +5 ppm) were fitted to a two-pool model of free water and MT. Six variables were estimated between pre-determined bounds: the $T_{1,obs}$ and $T_{2,obs}$ of the free water, and the size, exchange rate, apparent T_2 and peak position of the MT pool ($M_{0,b}$, k_b and $T_{2,b}$, $\delta\omega_b$); $T_{1,f}$ was fixed at 2 s, and here we assumed that $T_{1,b}$ could be fixed at 2 s (assuming a small bound pool size¹⁵). Next, a three-pool model of free water, MT, and amide was fitted to the acquired z-spectra excluding points between 2 to 1 ppm and -1 to -5 ppm, for the four variables describing the amide pool ($M_{0,c}$, k_c and $T_{2,c}$, $\delta\omega_c$), while fixing the six parameters for the free water and MT pools to the results from the previous fit. This was repeated for each pool in turn to give estimates for the sizes of each peak. Subsequently the fits were repeated to all datapoints, for the four variables of each pool in turn, taking the parameters describing the other peaks from the previous fits to account for the effects of overlapping peaks. Finally, the entire measured z-spectrum was fitted to a model including all exchanging pools and using the latest fitted values for the variables of each exchanging pool as starting values in the fit.

We also investigated the effect on the final fit of dropping pools from the model.

4 | RESULTS

4.1 | Z-PSO optimisation and testing

Figure 2A shows that the computational time for the PSO increased linearly with the number of particles used (in a single swarm), but the sum of squares of the residuals (SSR) declined approximately exponentially, with little benefit of using more than 1000 particles for this model. Figure 2B shows how repeating the fit with new swarms gradually identified better fits with smaller SSRs (at the fifth and 63rd fits for Figure 3B). Figure 2C

shows if fits were repeated at different swarm sizes to give the same total number of particles; swarm size had little effect on the total computation time (wall clock time), and the goodness of fit did not change significantly with swarm size, although even the smallest of swarms were better at finding a smaller SSR than a series of individual particles.

Figures 3 and S1 show the results of fitting simulated noisy data from a simple two-pool (amide + free water) system. The results suggest that the fit provides high precision and accuracy both for pool size and exchange rate, except for some slow exchange rate cases, particularly when

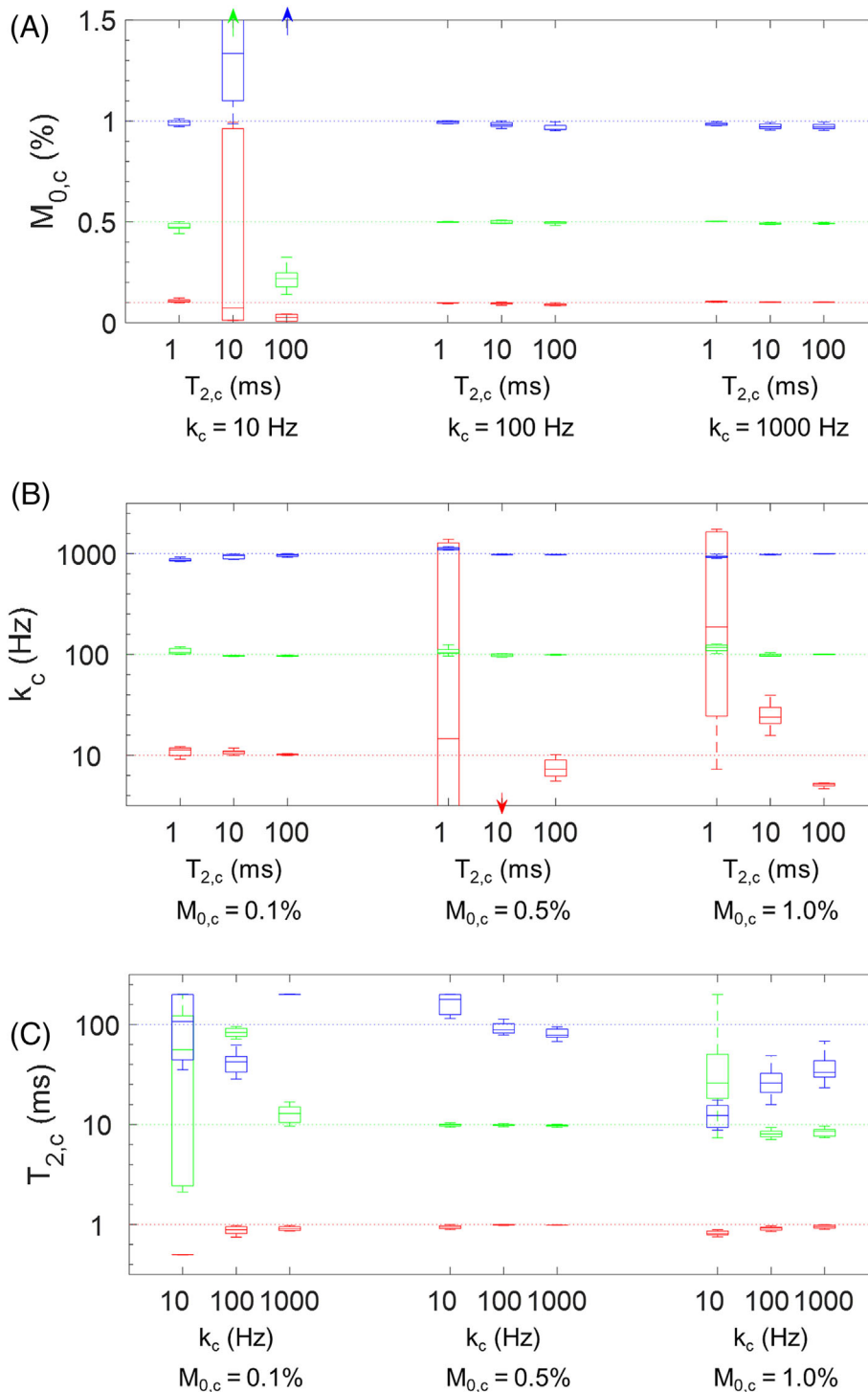


FIGURE 3 Monte Carlo fits of noisy simulated two-pool (amide + free water) data for the amide (A) Pool size, (B) Exchange rate, and (C) $T_{2,c}$. The boxes indicate the mean and standard deviation of the fitted results. The colours and corresponding dotted lines indicate the different simulated parameters for the amide pool.

$T_{2,c}$ is short, which is expected, as short $T_{2,c}$ and low exchange rate both broaden the peak. Overall $T_{2,c}$ can also be fitted but with some variability, particularly at higher values (~ 100 ms).

Figures 4 and S2 show that when an underlying MT pool was included (i.e., MT, amide, and free water pools) the fit was robust for both the MT and CEST parameters, with significant systematic or random errors only for small MT concentration ($M_{0,b} = 1\%$) and low exchange rate ($k_b = 1$ Hz).

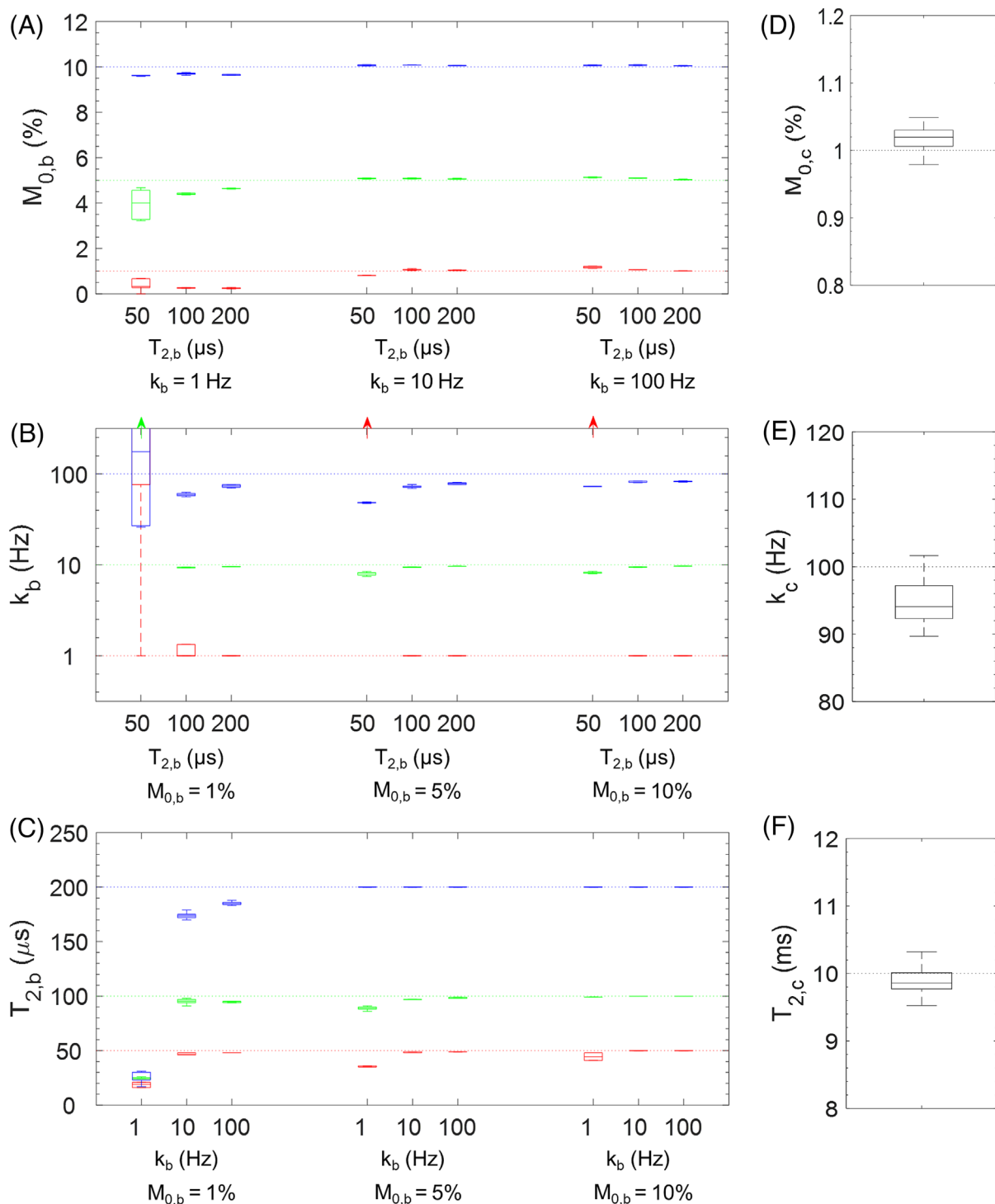


FIGURE 4 Monte Carlo fits of noisy simulated three-pool (MT, amide + free water) data for the MT (A) Pool size, (B) Exchange rate, and (C) $T_{2,b}$, along with (D) Pool size, (E) Exchange rate, and (F) $T_{2,c}$ fitted for the fixed amide pool. The boxes indicate the mean and standard deviation of the fitted results. The colours and corresponding dotted lines indicate the different simulated values of pool parameters. MT, magnetisation transfer.

4.2 | Creatine phosphors

Table 2 and Figure S3 give the fitted parameters for the creatine phantom scanned at different pH and temperatures, with Figure 5 highlighting that the creatine–water exchange rate was highly dependent on temperature but independent of pH in this experiment.

4.3 | Human brain tissue in vivo

Figure 6 shows that the z-PSO fitted in vivo in human GM and WM z-spectra well in most cases (raw images are shown in Figure S4). Table 3 shows the parameters fitted to the six-pool model, averaged over all subjects, and indicates when a significant difference was found between the GM and WM values.

We compared the results from the six- and five-pool models (excluding each exchanging pool in turn). We found the results for each five-pool model agreed with the six-pool model within two standard deviations of the variation across the group, except: (1) when $\text{NOE}_{-3.5\text{ppm}}$ was excluded, in which case $\text{NOE}_{-1.7\text{ppm}}$ was estimated to be significantly larger for GM; (2) when the amide pool was excluded, in which case the adjacent amine pool size was estimated to be larger than expected, and the $\text{NOE}_{-1.7\text{ppm}}$ pool was estimated to be larger in WM, probably because of the overlap across the water peak; and (3) when MT was excluded all pools were estimated to be larger, as expected, except for $\text{NOE}_{-1.7\text{ppm}}$.

We used an F-test to determine whether the six-pool model was significantly better than the five-pool model for each subject individually (Figure S5 shows the fits for one subject). The fit to the six-pool model was significantly better for all subjects, except for when (1) amide was missed: the F-test suggested that the six-pool model was a significantly better fit for 50% of subjects at p less than 0.05 (33% at $p < 0.01$) for GM and for 17% of subjects at p less than 0.05 (50% at $p < 0.1$) for WM, although Figure 6 shows clear peaks in the data at 3.5 ppm for all subjects; (2) $\text{NOE}_{-1.7\text{ppm}}$ was missed: the six-pool model was a significantly better fit in 67% of cases at p less than 0.01 in both GM and WM; (3) amine was missed: the six-pool model was significantly better in 83% of subjects at p less than 0.05 (66% at $p < 0.01$) for both GM and WM. Subject 2 had twice the sum of square error compared with other subjects and was one of the subjects that showed no improvement in the six-pool

TABLE 2 Results of fitting the z-spectra from the creatine phantom with the z-PSO algorithm. The fitted $T_{1\text{obs}}$ was between 1960 and 2070 ms with T_{1f} fixed at 2 s, while the fitted T_{2f} varied between 0.5 and 2 s (full results are shown in Figure S3).

	10°C			20°C			30°C			40°C		
	$M_{0,c}$ (%)	k_c (Hz)	$T_{2,c}$ (ms)	$M_{0,c}$ (%)	k_c (Hz)	$T_{2,c}$ (ms)	$M_{0,c}$ (%)	k_c (Hz)	$T_{2,c}$ (ms)	$M_{0,c}$ (%)	k_c (Hz)	$T_{2,c}$ (ms)
pH 5.5	0.50	17	>100	0.26	117	15.8	0.29	261	>100	0.31	658	28.6
pH 7.0	0.50	22	>100	0.35	104	9.9	0.29	300	23.6	0.31	689	>100
pH 8.5	0.31	37	>100	0.20	159	12.9	0.17	329	>100	0.14	676	13.4

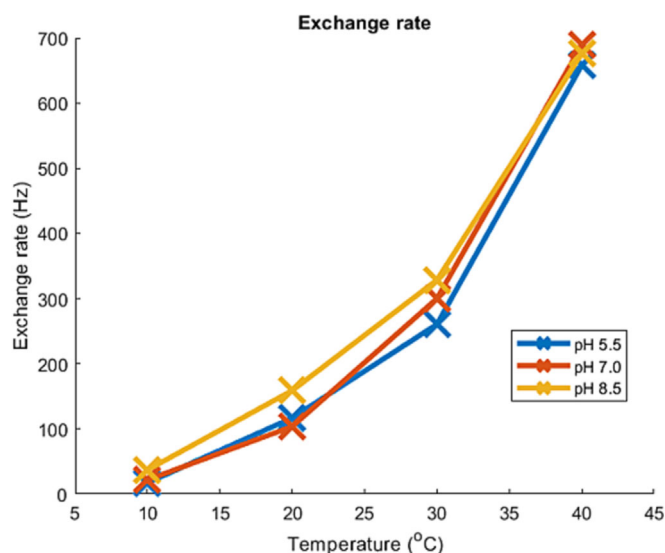


FIGURE 5 Variation of measured exchange rate with pH and temperature for the creatine phosphors.

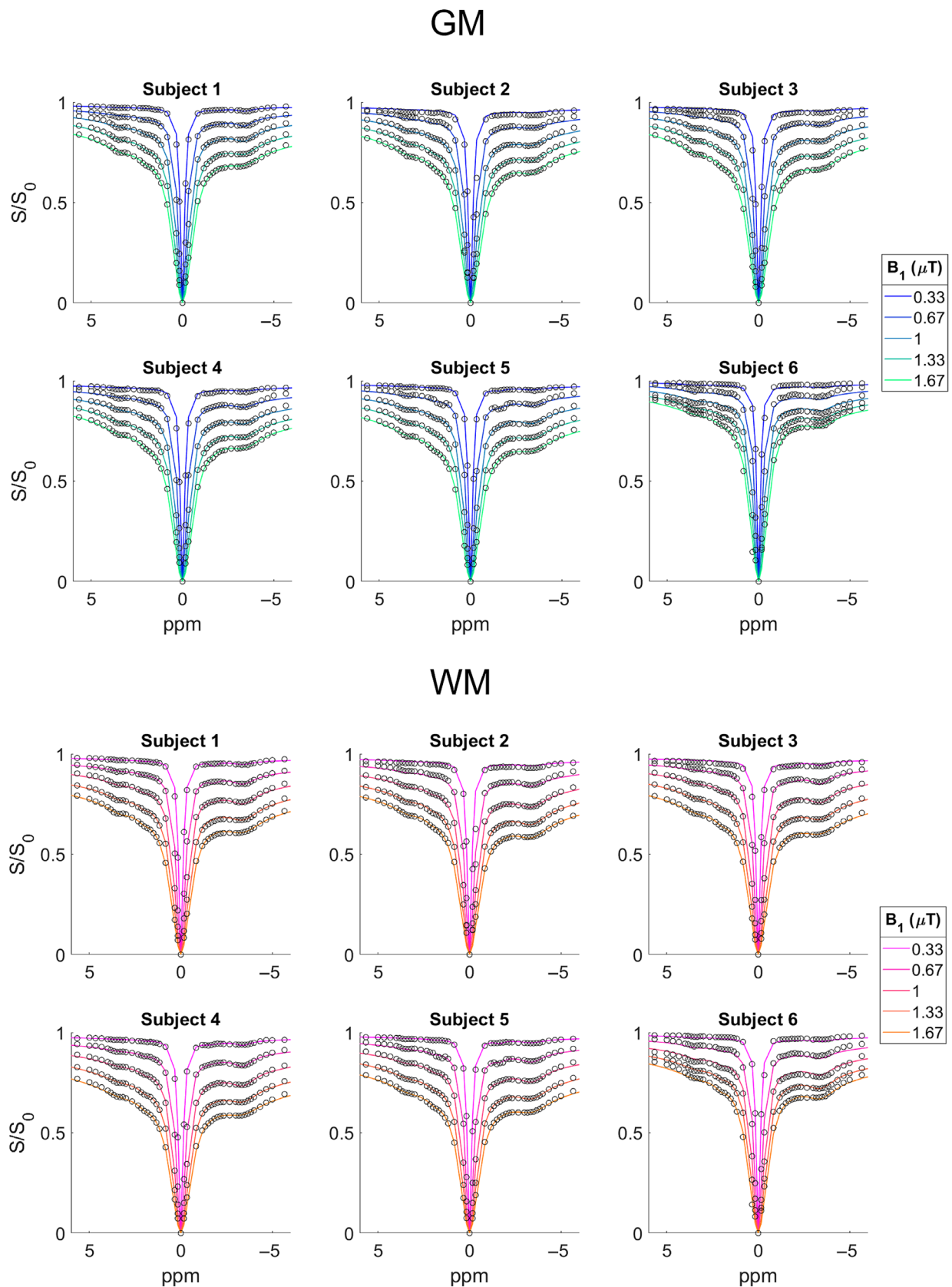


FIGURE 6 In vivo z-spectra for grey matter (GM; blue) and white matter (WM; red) for six subjects (data shown as points and best fits shown as lines).

TABLE 3 Parameters resulting from fitting in vivo human grey matter (GM) and white matter (WM) z-spectra to the five-pool model. The results quoted are the intersubject mean and standard deviation. The GM and WM results are compared with a two tailed t-test.

		MT	Amides	Amines	NOE _{-3.5ppm}	NOE _{-1.7ppm}
M ₀ (%)	GM	5.1 ± 0.4	0.17 ± 0.07	0.04 ± 0.01	0.26 ± 0.06	0.1 ± 0.1
	WM	7.1 ± 0.6	0.11 ± 0.04	0.03 ± 0.01	0.42 ± 0.04	0.7 ± 0.8
	t-test	* <i>p</i> = 0.00008	<i>p</i> = 0.08	<i>p</i> = 0.1	* <i>p</i> = 0.0002	<i>p</i> = 0.1
k (Hz)	GM	6 ± 2	145 ± 80	298 ± 215	68 ± 63	78 ± 100
	WM	8 ± 3	176 ± 156	191 ± 48	34 ± 13	42 ± 70
	t-test	<i>p</i> = 0.35	<i>p</i> = 0.7	<i>p</i> = 0.3	<i>p</i> = 0.2	<i>p</i> = 0.5
T ₂ (ms)	GM	0.09 ± 0.02	0.53 ± 0.05	3 ± 1	0.90 ± 0.15	1.4 ± 0.3
	WM	0.080 ± 0.009	0.69 ± 0.16	4 ± 1	0.93 ± 0.18	7 ± 11
	t-test	<i>p</i> = 0.1	<i>p</i> = 0.04	<i>p</i> = 0.51	<i>p</i> = 0.8	<i>p</i> = 0.3

*Significant difference at *p* < 0.01.

model in these three cases, possibly because the water peak was broader compared with the other subjects. Subject 6's data were acquired at lower power, which may explain why the NOE_{-1.7 ppm} and amide peaks made no difference in that case.

5 | DISCUSSION

We have estimated pool size, T₂ and exchange rate for MT, amide, amine, and two NOE z-spectrum components, fitting large z-spectrum datasets using PSO with limited dependence on the starting points in the fit. There are few prior reports of these parameters being measured simultaneously because of the large datasets required and the difficulty in fitting the data, but they are potentially of biomedical interest, for instance, in assessing demyelination and remyelination in multiple sclerosis, amides in tumours, or pH in tumours or after stroke. They are also important in optimising future experiments because there is considerable interaction between the exchange rate and the dependence of the observed z-spectrum on B₁ amplitude. The results are also relevant at lower field because exchange rate and fundamental pool size are B₀ independent and knowledge of T₂ at 7T will guide the values likely to occur at lower field.

To achieve a fit in a reasonable time we fitted the analytical solution to the Bloch–McConnell equations, which requires the z-spectra to be acquired using CW (or approximate CW) saturation, which we implemented using alternating transmission on a dual channel system. This will only be approximate in some parts of the head, but it has been shown that pulsed irradiation may be a suitable alternative to CW saturation when measuring samples containing only slow exchanging pools.²⁷

5.1 | Z-PSO fitting for multipower z-spectra

The PSO performed well using many small swarms compared with one large swarm, which allowed parallelisation to drastically reduce the fitting time. Nonetheless, a small PSO fitted better than one particle repeated 100,000 times (equivalent to a simple least-squares fit repeated for multiple starting points; Figure 2C), showing the power of the collective search approach. The University of Nottingham High Performance Computing system allows a maximum of 400 parallel computations per user, and therefore, by using 100 repeats of 1000 particle swarms, we could fit z-spectra datasets acquired at five RF powers together in about 16 min. It is not clear why the 100,000 particle fit (Figure 2C) was so much slower, but this may have been due to the high memory demand for the large particle swarm or greater communications between the particles.

Monte Carlo simulations (Figures 3 and 4) confirmed that pool size, exchange rate, and T₂ can be estimated accurately and precisely for a two-pool model, provided that T₂ is not too long and the exchange rate is not too slow. It is difficult to fit pools with low exchange rates, particularly for short T₂, as these situations both give low amplitude peaks (Figures 3 and S1). However, the exchange rate is generally considered on a logarithmic scale, so even a 100% error can provide a useful guide to the physical value. Longer T₂ values can be difficult to fit as the line width becomes dominated by exchange processes so that T₂ has little effect on the spectra (Figure S1). Figures 4 and S2 show that for a three-pool system the PSO could fit the MT pool well, except when the pool size was small, the exchange rate was slow, or T₂ was very short, as in these cases the parameter would have very little impact on the spectrum.

The primary strength of the z-PSO is its inherent lack of sensitivity to starting values (including B₁) and hence lack of bias in the results, which will be particularly valuable when applying this technique in clinical conditions where exchange rates and pool sizes may change considerably both temporally and spatially because of physiological changes in pH, temperature, and tissue composition. The alternative approach is to use

fingerprinting and machine learning approaches^{7,8} which require prior simulation of a very large library of z-spectra⁹ incorporating all possible physiological and physical conditions, potentially trading memory for computational time. A head-to-head comparison of these methods in real-world clinical scenarios is needed.

5.2 | Creatine phantom

The creatine exchange rate was found to decrease exponentially with temperature as expected and it agreed reasonably well with previous reports.²⁸ Varying pH using a phosphate buffer had no measurable effect on the measured exchange rate of the samples (Figures 5 and S3). However, a recent study suggests that creatine exchange is not strongly catalysed by phosphate,²⁹ and another study has shown a complex relationship between line broadening and phosphate,³⁰ which is similar to the changes we see in our data, as demonstrated in Figure S3c.

The concentration of creatine used was 76 mM, and the molarity of water is 55.56 M. Assuming four protons per mole for creatine and two protons per mole for water, then the fitted pool size is expected to be 0.26% for these solutions (assuming all the creatine protons are NMR-visible in the regime of the experiment). This agrees well with the results, particularly at high temperature (i.e., high exchange rate), but somewhat larger values were observed at low temperature (i.e., low exchange rate), consistent with the scatter observed for a low exchange rate in Figure 3.

The fitted $T_{2,c}$ sometimes hit the upper bound of 100 ms used in these simulations, but when it fitted it generally approximated the literature value of 30 ms.²⁸ This variability is also predicted in the simulation results in Figure 3.

The $T_{1,obs}$ did not vary very much around the fixed $T_{1,f}$ value of 2000 ms. We also investigated the effect of allowing $T_{1,f}$ to vary with temperature (from 2500 to 4000 ms between 10 and 40°C³¹) and the overall results for pool size and exchange rate were very similar, although the exchange rate at 40°C reduced slightly to around 550 Hz.

5.3 | Human brain tissue in vivo

We successfully fitted the in vivo z-spectra acquired at multiple B_1 values to a Bloch-McConnell six-pool model (Table 3). We averaged over the whole of the GM and WM, but the regions could be subdivided.

The observed spectra and F-test results together suggest that six pools are required to describe in vivo 7T brain data acquired in this B_1 range, and the parameters fitted to five-pool models generally agreed with the parameters fitted to the six-pool model. To compare these results with the literature, we have reviewed studies that have quantified the pool size or exchange rates for at least three pools in Table 4. We have not included many other studies that have quantified pool sizes in the z-spectra but may have been confounded by the effects of multiple exchanging pools. For instance, SIR and omega plots³³ methods provide convenient and robust measures of pool size and exchange rate, respectively, but can be sensitive to several exchanging pools. Such measures are invaluable in certain circumstances (e.g., for assessing changes in pH), but the fitted parameters cannot then be compared with the pool-specific values measured here.

We confirmed that the MT pool is larger in WM than in GM (Table 3), which is assumed to be due to myelin. Here, we assumed that T_{1b} could be neglected in the model and it was fixed at 2 s; this is not valid for large MT pool sizes and non-Lorentzian line shapes. The measured MT pool sizes are similar in absolute and relative terms to those measured in the literature.^{9,32} Larger values (up to about double, particularly in WM) are sometimes reported,^{7,8,16,34} often from models assuming only one or two exchanging pools or with limited freedom on the parameters of the other pools,^{7,35-37} so that results for the MT pool are probably influenced by more than just the solid-state pool. There is considerable variability in the values of exchange rate and T_2 reported for the bound pool in the literature, probably because of differences in the line shape assumed for this pool, different saturation powers used, and the difficulty of separating T_2 and the exchange rate given that they have counteracting effects on the line width. However, we and Liu et al.³² measured similar values of T_2 and both groups assumed a Lorentzian line shape and sampled over a similar frequency range, although Liu et al. used a larger range of saturation powers, which may explain why we measured different exchange rates. Some of these variations could be reduced by making fewer assumptions for the bound pool model (i.e., by using eq. 10 from Zaiss et al.² rather than eq. 16 from Zaiss and Bachert¹⁵).

There has been less work on quantification of the NOE_{-3.5ppm} pool; however, our pool size fraction is much smaller than that previously reported (Table 3), possibly because of the long T_2 fitted. It was found to be significantly larger in WM than in GM, confirming previous reports that have attributed this difference to myelin.

The second NOE pool located at -1.7 ppm has previously been identified in blood and the sagittal sinus,²¹ rat brain,²⁶ and brain tumours,³⁸ but has not been fully quantified in the healthy human brain. We found that the pool size is significantly higher in WM than in GM, and it has been speculated that this may be indicative of mobile membrane proteins.³⁹

We found a trend for a larger amide pool in GM than in WM, agreeing with previous reports, with similar relative differences in amplitudes.⁴⁰ The T_2 values measured for this pool were smaller than those reported by Heo et al.,⁸ and both are an order of magnitude smaller than those reported by Liu et al.,³² although in all three studies the exchange rates are of the same order. Again, it is difficult to separate these parameters

TABLE 4 Review of previous measurements of key parameters in the z-spectrum in the human brain in vivo.

Ref.	MT				Amide proton transfer					
	M_{0b} GM %	M_{0b} WM %	k_b GM (Hz)	k_b WM (Hz)	T_2 GM (μ s)	T_2 WM (μ s)	M_{0c} GM %	M_{0c} WM %	k_c GM (Hz)	k_c WM (Hz)
This paper	5.4 ± 0.4	7.2 ± 0.5	6 ± 2	7 ± 3	90 ± 10	80 ± 9	0.17 ± 0.07	0.10 ± 0.06	130 ± 80	260 ± 180
⁹	4.4 ± 0.4	8.9 ± 0.3	50^a	50^a	9^a	9^a	0.20 ± 0.02	0.21 ± 0.03	200^a	200^a
³²	3.4 ± 0.4	6.2 ± 0.4	63.5 ± 4.5	67.5 ± 7.0	104 ± 4	84 ± 2	0.25 ± 0.05	0.22 ± 0.04	282.9 ± 0.9	281.2 ± 0.6
⁷	10.6 ± 1.5	16.9 ± 1.3	12.5 ± 2.0	10.3 ± 0.9	45.0 ± 1.5	47 ± 1	12 ± 1	11.5 ± 0.7		
⁸	6.3 ± 0.7	11.2 ± 0.7	40 ± 6	29 ± 5	67 ± 5	63 ± 4	266 ± 22 mM	212 ± 22 mM	365 ± 19	162 ± 16
	M	M								

Abbreviations: GM, grey matter; MT, magnetisation transfer; NOE, nuclear Overhauser enhancement; WM, white matter.

^aA value that was assumed in the model (rather than fitted for).**TABLE 4** (Continued)

Ref.	Amide proton transfer		NOE		k_r GM (Hz)	k_r WM (Hz)	T_2 GM (μ s)	T_2 WM (μ s)	B_0 (T)	# B1 levels	# offset freq	# pools exch. with water
	T_2 GM (ms)	T_2 WM (ms)	M_{0n} GM %	M_{0n} WM %								
This paper	0.54 ± 0.07	0.75 ± 0.01	0.25 ± 0.05	0.42 ± 0.05	70 ± 60	37 ± 10	840 ± 40	850 ± 40	7	N = 5 0.33–1.33 μ T for 3 s	46	5
⁹	10^a	10^a	3.0 ± 0.1	5.0 ± 0.1	10^a	10^a	300^a	300^a	7	N = 3 0.33–1.25 μ T for 1.2 s	15	3
³²	29 ± 7	23 ± 6	1.2 ± 0.2	2.4 ± 0.2	24 ± 2	27 ± 2	402 ± 26	318 ± 7	7	N = 6 0.2–2.3 μ T (or N = 7 0.2–4.7 μ T) for 4 s	34	3
⁷			12.7 ± 0.7	12.7 ± 0.6					3	N = 1 1.2 μ T for 2 s	16	3
⁸	1.1 ± 0.4	2.1 ± 0.3							3	N = 3 1–2 μ T	46 (asym)	3

Abbreviations: GM, grey matter; MT, magnetisation transfer; NOE, nuclear Overhauser enhancement; WM, white matter.

^aA value that was assumed in the model (rather than fitted for).

and the results are likely to depend on the saturation powers used, but it should be noted that we also fitted for amine pool, which may otherwise contaminate the amide fit.

The pool labelled as amines (at 2 ppm) was measured as having the fastest exchange rate, as expected, but was still lower than generally assumed in some work,⁴¹ although this pool may correspond to several metabolites with different exchange rates.^{42,43} However, the slow exchange rate measured in the amines group, and the fast exchange rate of the amide group, may also indicate contributions from an underlying aromatic NOE, reported to be at +1 to +5 ppm.⁴⁴

Others have reported a CEST signal at 3 ppm which has generally been related to glutamine in the brain, but its higher exchange rate makes it inaccessible with the saturation powers generally available on human scanners and so we did not attempt to fit for it.

The z-spectrum contains contributions from a range of metabolites and a large range of data is required to assess pools, particularly if they have very different exchange rates. However, such large datasets are very susceptible to experimental errors and variations. The in vivo data in Table 3 show more variability than the simulations might predict, and although this could be due to genuine biological variability, it seems likely that it is driven by variations in the experimental conditions, for instance, low B_1 (subject 6), apparently long water T_2 (subject 2), or variations in T_1 . Moreover, some variation in the experimental and biophysical parameters will occur across the ROI and it is possible more stable results could be achieved with smaller ROIs. Overall, the largest % variation occurred in the NOE-1.7 ppm peak, probably related to its small amplitude, but also its closeness to the water peak and hence its sensitivity to small variations in B_0 and direct saturation. The dependence of the fit on so many experimental and biophysical parameters is a weakness of the approach; future work should explore the sensitivity of the final results to these parameters to identify strategies for reducing variability.

In future, better sensitivity could be obtained by combining methods where the amplitude and length of saturation are modified to enhance sensitivity to fast or slow exchange pools,^{5,41,45} although that would require a change to the analytical expression used in the fit which currently assumed CW steady state saturation.⁶ Here, the imaging readout module gave a relatively high spatial resolution, but the scan time could be reduced, for instance, by using an EPI readout.

6 | CONCLUSIONS

We have used PSO to fit multipower CEST spectra to characterise the properties of the amide, amine, NOE_{-3.5ppm} and NOE_{-1.7ppm} pools in GM and WM at 7T. The approach was validated using simulations and a creatine phantom at various temperatures.

ACKNOWLEDGEMENTS

Andrew Carradus held a studentship with the Haydn Green Foundation. We are grateful for access to the University of Nottingham's Augusta HPC service. We are also grateful for the work of both Andrew Peters and Hans Hoogduin and colleagues for their work and help on the 7T Philips scanner platform for us to successfully run the semi-CW saturation in vivo.

ORCID

Olivier E. Mougín  <https://orcid.org/0000-0001-9675-3530>

REFERENCES

1. Zhou J, Payen JF, Wilson DA, Traystman RJ, Van Zijl PCM. Using the amide proton signals of intracellular proteins and peptides to detect pH effects in MRI. *Nat Med*. 2003;9(8):1085-1090. doi:10.1038/nm907
2. Zaiss M, Zu Z, Xu J, et al. A combined analytical solution for chemical exchange saturation transfer and semi-solid magnetization transfer. *NMR Biomed*. 2015;28(2):217-230. doi:10.1002/nbm.3237
3. Zaiss M, Xu J, Goerke S, et al. Inverse Z-spectrum analysis for spillover-, MT-, and T1-corrected steady-state pulsed CEST-MRI—application to pH-weighted MRI of acute stroke. *NMR Biomed*. 2014;27(3):240-252. doi:10.1002/nbm.3054
4. Zaiss M, Bachert P. Chemical exchange saturation transfer (CEST) and MR Z-spectroscopy in vivo: a review of theoretical approaches and methods. *Phys Med Biol*. 2013;58(22):R221-R269. doi:10.1088/0031-9155/58/22/R221
5. McMahon MT, Gilad AA, Zhou J, Sun PZ, Bulte JWM, Van Zijl PCM. Quantifying exchange rates in chemical exchange saturation transfer agents using the saturation time and saturation power dependencies of the magnetization transfer effect on the magnetic resonance imaging signal (QUEST and QUESP): pH calibration for poly. *Magn Reson Med*. 2006;55(4):836-847. doi:10.1002/mrm.20818
6. Zaiss M, Angelovski G, Demetriou E, McMahon MT, Golay X, Scheffler K. QUESP and QUEST revisited—fast and accurate quantitative CEST experiments. *Magn Reson Med*. 2018;79(3):1708-1721. doi:10.1002/mrm.26813
7. Kim B, Schär M, Park HW, Heo HY. A deep learning approach for magnetization transfer contrast MR fingerprinting and chemical exchange saturation transfer imaging. *Neuroimage*. 2020;221:117165. doi:10.1016/j.neuroimage.2020.117165
8. Heo HY, Han Z, Jiang S, Schär M, van Zijl PCM, Zhou J. Quantifying amide proton exchange rate and concentration in chemical exchange saturation transfer imaging of the human brain. *Neuroimage*. 2019;189:202-213. doi:10.1016/j.neuroimage.2019.01.034
9. Geades N, Hunt BAEE, Shah SM, Peters A, Mougín OE, Gowland PA. Quantitative analysis of the z-spectrum using a numerically simulated look-up table: application to the healthy human brain at 7T. *Magn Reson Med*. 2017;78(2):645-655. doi:10.1002/mrm.26459

10. Chappell MA, Donahue MJ, Tee YK, et al. Quantitative Bayesian model-based analysis of amide proton transfer MRI. *Magn Reson Med*. 2013;70(2):556-567. doi:10.1002/mrm.24474
11. Eberhart R, Kennedy J. New optimizer using particle swarm theory. In: *Proceedings of the International Symposium on Micro Machine and Human Science*; 1995. doi:10.1109/mhs.1995.494215
12. Shi Y, Eberhart R. Modified particle swarm optimizer. In: *Proceedings of the IEEE Conference on Evolutionary Computation, ICEC*; 1998. doi:10.1109/icec.1998.699146
13. Poli R. Analysis of the publications on the applications of particle swarm optimisation. *J Artif Evol Appl*. 2008;2008:1-10. doi:10.1155/2008/685175
14. Hassan R, Cohanim B, De Weck O, et al. *A Comparison of Particle Swarm*. American Institute of Aeronautics and Astronautics; 2004.
15. Zaiss M, Bachert P. Exchange-dependent relaxation in the rotating frame for slow and intermediate exchange—modeling off-resonant spin-lock and chemical exchange saturation transfer. *NMR Biomed*. 2013;26(5):507-518. doi:10.1002/nbm.2887
16. Stanisiz GJ, Odrobina EE, Pun J, et al. T1, T2 relaxation and magnetization transfer in tissue at 3T. *Magn Reson Med*. 2005;54(3):507-512. doi:10.1002/mrm.20605
17. Haris M, Singh A, Cai K, et al. A technique for in vivo mapping of myocardial creatine kinase metabolism. *Nat Med*. 2014;20(2):209-214. doi:10.1038/nm.3436
18. Sun PZ, Xiao G, Zhou IY, Guo Y, Wu R. A method for accurate pH mapping with chemical exchange saturation transfer (CEST) MRI. *Contrast Media Mol Imaging*. 2016;11(3):195-202. doi:10.1002/cmml.1680
19. Hoogduin H, Khlebnikov V, Keupp J, et al. Semi continuous wave CEST with alternating sets of 4 transmit channels at 7T. *MAGMA*. 2017;30(Suppl 1):S1-S152. doi:10.1002/nbm.3687
20. MathWorks, Inc. MATLAB, version 9.6. Published online 2019. www.mathworks.com/products/matlab
21. Shah SM, Mougou OE, Carradus AJ, et al. The z-spectrum from human blood at 7T. *Neuroimage*. 2018;167:31-40. doi:10.1016/j.neuroimage.2017.10.053
22. Greene DJ, Koller JM, Hampton JM, et al. Behavioral interventions for reducing head motion during MRI scans in children. *Neuroimage*. 2018;171:234-245. doi:10.1016/j.neuroimage.2018.01.023
23. Mougou O, Abdel-Fahim R, Dineen R, Pitiot A, Evangelou N, Gowland P. Imaging gray matter with concomitant null point imaging from the phase sensitive inversion recovery sequence. *Magn Reson Med*. 2016;76(5):1512-1516. doi:10.1002/mrm.26061
24. FAST—FslWiki. Accessed April 12, 2022. <https://fsl.fmrib.ox.ac.uk/fsl/fslwiki/FAST>
25. MCFLIRT—FslWiki. Accessed April 12, 2022. <https://fsl.fmrib.ox.ac.uk/fsl/fslwiki/MCFLIRT>
26. Zhang XY, Wang F, Afzal A, et al. A new NOE-mediated MT signal at around -1.6 ppm for detecting ischemic stroke in rat brain. *Magn Reson Imaging*. 2016;34(8):1100-1106. doi:10.1016/j.mri.2016.05.002
27. Tee YK, Khrapitchev AA, Sibson NR, Payne SJ, Chappell MA. Evaluating the use of a continuous approximation for model-based quantification of pulsed chemical exchange saturation transfer (CEST). *J Magn Reson*. 2012;222(3):88-95. doi:10.1016/j.jmr.2012.07.003
28. Goerke S, Zaiss M, Bachert P. Characterization of creatine guanidinium proton exchange by water-exchange (WEX) spectroscopy for absolute-pH CEST imaging in vitro. *NMR Biomed*. 2014;27(5):507-518. doi:10.1002/nbm.3086
29. Yao J, Wang C, Ellingson BM. Influence of phosphate concentration on amine, amide, and hydroxyl CEST contrast. *Magn Reson Med*. 2021;85(2):1062-1078. doi:10.1002/mrm.28481
30. Lee JS, Regatte RR, Jerschow A. Bloch equations for proton exchange reactions in an aqueous solution. *Concepts Magn Reson Part A Bridg Educ Res*. 2016;45A(3):e21397. doi:10.1002/CMR.A.21397
31. Tsukiashi A, Min KS, Kitayama H, et al. Application of spin-crossover water soluble nanoparticles for use as MRI contrast agents. *Sci Rep*. 2018;8(1):1-5. doi:10.1038/s41598-018-33362-6
32. Liu D, Zhou J, Xue R, Zuo Z, An J, Wang DJJ. Quantitative characterization of nuclear Overhauser enhancement and amide proton transfer effects in the human brain at 7 Tesla. *Magn Reson Med*. 2013;70(4):1070-1081. doi:10.1002/mrm.24560
33. Wang Z, Shaghghi M, Zhang S, et al. Novel proton exchange rate MRI presents unique contrast in brains of ischemic stroke patients. *J Neurosci Methods*. 2020;346:108926. doi:10.1016/j.jneumeth.2020.108926
34. Mougou O, Coxon R, Pitiot A, Gowland P. Magnetization transfer phenomenon in the human brain at 7 T. *Neuroimage*. 2010;49(1):272-281. doi:10.1016/j.neuroimage.2009.08.022
35. Ropele S, Seifert T, Enzinger C, Fazekas F. Method for quantitative imaging of the macromolecular 1H fraction in tissues. *Magn Reson Med*. 2003;49(5):864-871. doi:10.1002/mrm.10427
36. Dortch RD, Moore J, Li K, et al. Quantitative magnetization transfer imaging of human brain at 7T. *Neuroimage*. 2013;64:640-649. doi:10.1016/j.neuroimage.2012.08.047
37. Mckeithan LJ, Lyttle BD, Box BA, et al. 7T quantitative magnetization transfer (qMT) of cortical gray matter in multiple sclerosis correlates with cognitive impairment. *Neuroimage*. 2019;203:116190. doi:10.1016/j.neuroimage.2019.116190
38. Zu Z. Ratiometric NOE(-1.6) contrast in brain tumors. *NMR Biomed*. 2018;31(12):e4017. doi:10.1002/nbm.4017
39. Desmond KL, Moosvi F, Stanisiz GJ. Mapping of amide, amine, and aliphatic peaks in the CEST spectra of murine xenografts at 7 T. *Magn Reson Med*. 2014;71(5):1841-1853. doi:10.1002/mrm.24822
40. Sui R, Chen L, Li Y, Huang J, et al. Whole-brain amide CEST imaging at 3T with a steady-state radial MRI acquisition. *Magn Reson Med*. 2021;86(2):893-906. doi:10.1002/mrm.28770
41. Schmitz-Abecassis B, Vinogradov E, Wijnen JP, et al. The use of variable delay multipulse chemical exchange saturation transfer for separately assessing different CEST pools in the human brain at 7T. *Magn Reson Med*. 2022;87(2):872-883. doi:10.1002/MRM.29005
42. Haris M, Nanga RPR, Singh A, et al. Exchange rates of creatine kinase metabolites: feasibility of imaging creatine by chemical exchange saturation transfer MRI. *NMR Biomed*. 2012;25(11):1305-1309. doi:10.1002/nbm.2792
43. Xu J, Chung JJ, Jin T. Chemical exchange saturation transfer imaging of creatine, phosphocreatine, and protein arginine residue in tissues. *NMR Biomed*. 2022;36(6):e4671. doi:10.1002/nbm.4671
44. Jin T, Kim SG. In vivo saturation transfer imaging of nuclear Overhauser effect from aromatic and aliphatic protons: implication to APT quantification. *Proc Intl Soc Mag Reson Med*. 2012;205(2):1579. doi:10.1002/mrm.24315

45. Xu J, Chan KWY, Xu X, Yadav N, Liu G, van Zijl PCM. On-resonance variable delay multipulse scheme for imaging of fast-exchanging protons and semisolid macromolecules. *Magn Reson Med*. 2017;77(2):730-739. doi:[10.1002/mrm.26165](https://doi.org/10.1002/mrm.26165)

SUPPORTING INFORMATION

Additional supporting information can be found online in the Supporting Information section at the end of this article.

How to cite this article: Carradus AJ, Bradley JMP, Gowland PA, Mougín OE. Measuring chemical exchange saturation transfer exchange rates in the human brain using a particle swarm optimisation algorithm. *NMR in Biomedicine*. 2023;e5001. doi:[10.1002/nbm.5001](https://doi.org/10.1002/nbm.5001)